analytical chemistry

Subscriber access provided by Imperial College London | Library

Article

Capacitive sensing for monitoring of microfluidic protocols using nanolitre dispensing and acoustic mixing

Yaqi Zhang, Muhsincan Sesen, Alex de Marco, and Adrian Neild

Anal. Chem., **Just Accepted Manuscript** • DOI: 10.1021/acs.analchem.0c01906 • Publication Date (Web): 06 Jul 2020

Downloaded from pubs.acs.org on July 14, 2020

Just Accepted

"Just Accepted" manuscripts have been peer-reviewed and accepted for publication. They are posted online prior to technical editing, formatting for publication and author proofing. The American Chemical Society provides "Just Accepted" as a service to the research community to expedite the dissemination of scientific material as soon as possible after acceptance. "Just Accepted" manuscripts appear in full in PDF format accompanied by an HTML abstract. "Just Accepted" manuscripts have been fully peer reviewed, but should not be considered the official version of record. They are citable by the Digital Object Identifier (DOI®). "Just Accepted" is an optional service offered to authors. Therefore, the "Just Accepted" Web site may not include all articles that will be published in the journal. After a manuscript is technically edited and formatted, it will be removed from the "Just Accepted" Web site and published as an ASAP article. Note that technical editing may introduce minor changes to the manuscript text and/or graphics which could affect content, and all legal disclaimers and ethical guidelines that apply to the journal pertain. ACS cannot be held responsible for errors or consequences arising from the use of information contained in these "Just Accepted" manuscripts.

is published by the American Chemical Society. 1155 Sixteenth Street N.W., Washington, DC 20036

Published by American Chemical Society. Copyright © American Chemical Society. However, no copyright claim is made to original U.S. Government works, or works produced by employees of any Commonwealth realm Crown government in the course of their duties.

Capacitive sensing for monitoring of microfluidic protocols using nanolitre dispensing and acoustic mixing

Yaqi Zhang[1], Muhsincan Sesen[1,2,†], Alex de Marco[3,4*] and Adrian Neild[1*]

[1]Department of Mechanical and Aerospace Engineering, Monash University, Clayton, Victoria (Australia)
[2]Institute of Biological Chemistry, Biophysics and Bioengineering, Heriot-Watt University, Edinburgh, EH14 4AS, (United Kingdom)
[3]Department of Biochemistry and Molecular Biology, Monash University, Clayton, Victoria (Australia)
[4]ARC Centre of Excellence for Advanced Molecular Imaging (Australia)
* Corresponding authors: alex.demarco@monash.edu, adrian.neild@monash.edu

†Present address: Department of Bioengineering, South Kensington Campus, Imperial College London, SW7 2AZ, (United Kingdom)

Supporting information:

- System set up overview
- Capacitive sensor validation
- Movie of automated fluorescein dispensing via feedback control

Abstract

The development of protocols for bio/chemical reaction requires alternate dispensing and mixing steps. Whilst most microfluidic systems use the opening of additional parts of the channel to allow the ingress of fixed volumes of fluid, this requires knowledge of the protocol before the design of the chip. Our approach of using a microfluidic valve to regulate the flow into an initially empty cavity allows for on-chip protocol development and refinement. Mixing is provided by way of surface acoustic wave excitation; this high-frequency vibration causes steady-state streaming flows. We show that capacitive sensing can be used to measure fluid levels, even if multiple fluid types are used, such that nanolitre dispensing accuracy is achieved. Also, the capacitive readout can be used to establish mixing quality and to monitor temperature fluctuations. These capabilities allow for protocols to be conducted without optical assessment, and so will allow for multiplexing, such that reactions could be conducted, simultaneously, in multiple chambers across a chip.

1. Introduction

Integrated microfluidics reactors[1] incorporating reagent dispensing, mixing and detection capabilities allow complex bio/chemical reactions to be conducted at the micro-scale. Such miniaturisation offers superior reaction efficiency, precise sample manipulation and highly sensitive measurement, all of which are crucial for applications including single-cell analysis[2-4], proteomics[5] and nano-chemical synthesis.[6-7] Microfluidic reactors can be classified into two types, droplet-based and single-phase continuous flow. Through the use of two immiscible phases, individual and isolated droplets of one sample in a buffer can be produced. In these systems, each of these droplets acts as a reactor;[6-10] allowing for fast parameter mapping and detection. They offer excellent versatility stemming from precise manipulation possibilities and the ability to rapidly alter droplet composition.[11] However, as the reaction volume is defined by the size of the droplet, typically in the pico to nanolitre range, the complexity of the reactions that can be conducted, and the information extracted is limited.

In contrast to droplet-based approaches, microscale continuous flow reactors[12-17] handle larger reaction volumes, in the range of tens of nanoliters, this allows for more complex, multistage reactions to be conducted. However, two technical challenges need to be addressed in this volume range. The first is versatile and precise manipulation of reagents, the second is mixing the fluids in a regime where viscous forces dominate,[18] noting that mixing purely by diffusion is a long process which may cause spatial and temporal variation in the measurement. As such, both accurate flow control and a method for uniform mixing are required.[19] To tackle the first challenge micro valves[20-23] have been used on-chip to successively control access to an additional volume in the microfluidic channel, with each newly opened section prescribing the amount of new reagent that is added to the sample volume. By sequential operating the valves, and in doing so circulating the reagent around the channel, mixing occurs. Such rotary mixers are capable of mixing 5 nL sample in a few minutes.[14] As the channel geometry dictates the volumes of reagent dispensed, one issue is that protocols are hard-wired into the system with no capability of modification, secondly, the long time scale of rotary mixing imposes a maximum reaction volume.

To have the flexibility to develop protocols directly on a chip, previously, we designed an approach in which an initially empty chamber can be partially filled with successive reagents, the flow of which is valve controlled. Once dispensed the reagents are mixed using surface acoustic wave driven acoustic streaming. This approach means that the dispensed volumes are related to the time the valve is open, rather than integral to the geometry of the chip, and the mixing can be reduced to 5 s, even for volumes up to 153 *nL*.[24] However, in this system, there was no mechanism to provide feedback on either the amount of fluid dispensed into the chamber or the degree of mixing obtained. Whilst optical measurement could be used for both of these tasks, this imposes a limit on the number of chambers that could be used simultaneously, as visual access is needed to each of them, so a different approach is required.

Here, we present an automated integrated system consisting of single-layer valve for fluid dispensing and surface acoustic wave actuator for mixing, and which incorporates capacitive sensing[25-31] as a feedback mechanism. Such a sensor can be multiplexed and uses the same fabrication steps as the electrodes used for SAW generation. The result is a feedback control algorithm capable of reagent dispensing with 2 nL accuracy, whilst being versatile enough to

accurately measure the dispensed volume of different fluids. Besides, the surface acoustic wave mixing can be monitored to assess whether mixing is complete and to assess the temperature changes which occur during this process.

2. System principle

Figure 1 shows a schematic and the sequence of operation of the proposed system. The key features of the chip are a reaction chamber, which is initially empty, into which small volumes of fluid can be dispensed using a single layer valve. The volume of fluid dispensed is measured using electrodes positioned under the reaction chamber, whilst electrodes outside the chamber can be used to generate surface acoustic waves to mix the reagents. The chamber also has an exit channel to allow the egress of the air which initially fills the chamber and for washing steps between reactions.

Surface acoustic wave (SAW) induced streaming[32] was utilised to aid the mixing.[33-34] When the SAW encounters fluid on the substrate, the acoustic energy couples into the fluid approximately in the form of plane wave at Rayleigh angle. Due to energy being coupled into the fluid, the surface wave amplitude decays exponentially[35-36] and hence there is a spatial gradient in the pressure field which gives rise to momentum flux in the fluid (termed the Reynolds stress),[37] this acts to generate a steady fluid flow or acoustic streaming.[32] The degree of spatial variation in the sound field governs the strength of the streaming field, for example, large Reynolds stresses occur at the interface between a bubble and a solid surface,[38-41] at sharp points[42-43] or the edge of a vibrating membrane.[44] In the context of SAW mixing, the Reynolds stress can be raised by increasing the attenuation of the SAW, which in turn is achieved by an increase of frequency, however, in higher attenuation regimes the area over which the stresses are generated is reduced. Hence, a balance occurs between the magnitude of the stresses and their spatial spread, which determines the optimum frequency of operation for a given chamber area. In previous work, this was analysed, and it was found that for a chamber of the size used in this work, 70 MHz is a suitable actuation frequency.[24]

The capacitive sensor positioned under the chamber was formed by a pair of coplanar interdigital electrodes covered by an insulating layer. The capacitance between these electrodes can be calculated by:[28]

$$C = \frac{2\varepsilon_r \varepsilon_0 l}{\pi} ln\left[\left(1 + \frac{w}{a}\right) + \sqrt{\left(1 + \frac{w}{a}\right)^2 - 1}\right] \qquad (1)$$

where w represents the width of the electrode, a is half the gap between the neighbouring electrodes and l is the total length of the electrodes. The only value that does not depend on the geometry is the relative permittivity (ε_r) of the fluids that will fill the chamber, which is temperature and fluid composition dependent. In the absence of fluid on the electrodes, ε_r, has a value of 1.0006. When the cavity is filled, the air is displaced and the relative permittivity of the fluid should be used. This can be expected to be significantly higher than that of air, for example, in water the value is 78.4 at 293K. For a partially wetted set of electrodes, the total capacitance would be the sum of that from the wetted total length of the electrodes (using ε_r for the fluid) with that from the air covered electrodes. As such, for a fixed electrode geometry, at a constant temperature and fluid type, the capacitance changes linearly with the fluid level. However, if there are free ions in a solution added to the chamber, the ions

will migrate to the electrodes and form an electrical double layer (Debye layer). This can cause an increase in the capacitance with the electrostatic potential decaying exponentially.[45-46] If multiple fluid types are used, then the degree that this affects the measurement may vary between the fluids, and this can have a larger effect compared to the relative permittivity. To avoid errors in the way the capacitance is measured, when the initial calibration is performed, the whole chamber must be wetted using the calibration fluid. This leaves a thin film of fluid across the surface and as such the electrical double layer is constant. In operation, when a different fluid type is added, the bulk fluid change alters the capacitance, due to the different permittivity, but the pre-wetting means the surface charge effect remains unaltered over the time frame required to measure the volume.

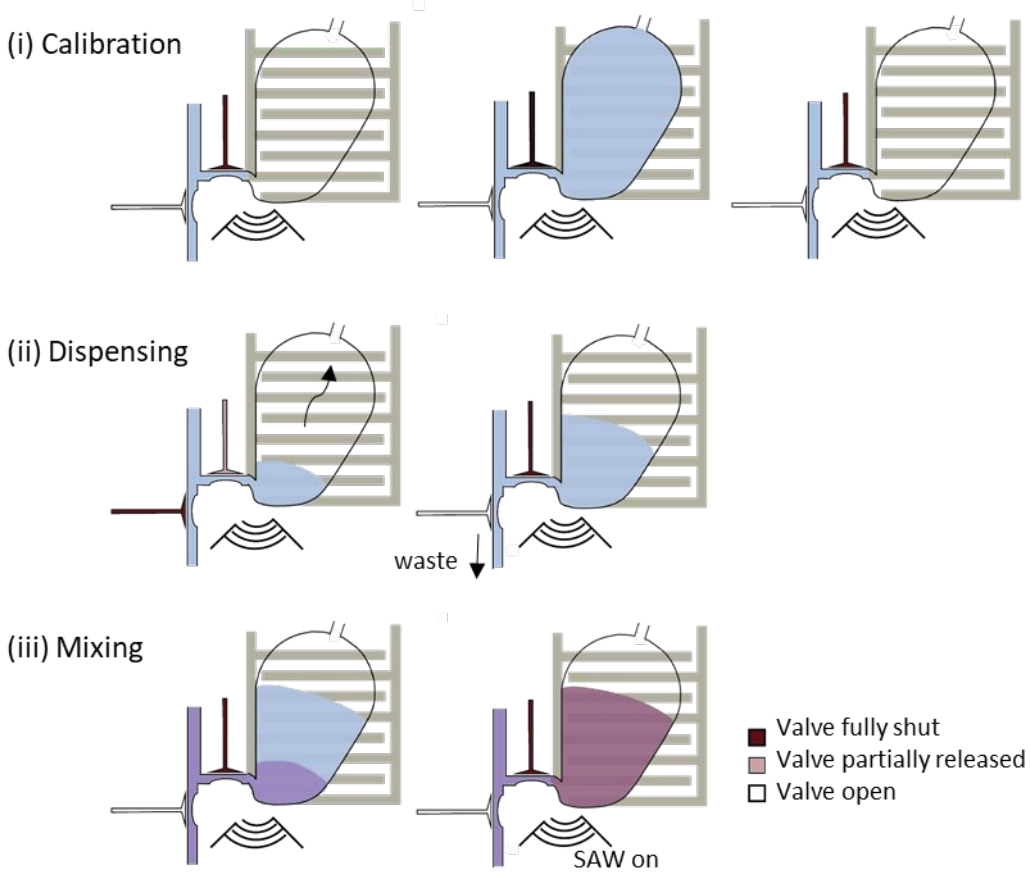

Figure 1 schematic and schematic and operation sequence of a microfluidic device consisting of the reaction chamber integrated with capacitive based fluid level sensor, single layer valve and IDT at the head of the chamber for rapid mixing. (i) Calibration of the capacitive sensor. (ii) Dispensing. (iii) Mixing: after the fluid was altered in the main channel and dispensed into the chamber, SAW was actuated at 70 MHz to aid the mixing process. The full experiment set up is depicted in Fig. S1.

3. Experimental

Fabrication

The device consists of two parts, the microfluidic channel which contains the reaction chamber and single layer valves were made of soft polydimethylsiloxane (PDMS; 1:20 ratio of curing agent and

polymer) and the Lithium Niobate piezoelectric substrate ($LiNbO_3$, 128° rotated Y-cut X propagating), on which the interdigital transducers (IDTs) and capacitive sensor are patterned. The master mould for the microfluidic channel, of 120 µm height, was fabricated through standard SU8 photolithography. The capacitive sensor and IDTs were patterned on the substrate via E-beam evaporation, starting with a 5 nm layer of Chromium for the adhesion layer, followed by a conductive layer. The conductive layer consists of 3 layers of alternating 20/40 nm Ti/Au deposition with 15 nm Ti finish to enhance adhesion with the passivation layer of SiO_2 (400 nm). The passivation layer not only provides insulation of the electrodes but also protect them from corrosion and cross-contamination. Focused IDTs (fIDTs) with a wavelength of 55 µm (operating at 68.8 MHz), an aperture of 240 µm and a focal point located 1000 µm away from the last finger pair were used in this work. The capacitive sensor under the reaction chamber was designed as straight IDTs with 80 µm in pitch (to avoid crosstalk with the fIDTs), 1260 µm in aperture and 23 sets of finger pairs.

To enhance the bonding between the membrane and substrate, such that it was capable of withstanding the high pressure applied to the single-layer valve, 10 µm PDMS was spin-coated onto the substrate. However, this layer was patterned, as it was found that when it was present above the capacitive sensor electrodes the PDMS layer compromised the accuracy of the measurement. This patterning was achieved by the use of first contact (Photonic Cleaning Tech, Platteville, USA) to cover the sensor electrodes during spin coating and then subsequently removed. Once the spin-coated PDMS was cured on a hot plate (70 °C for 30 mins), the substrate was ready for plasma bonding to the PDMS component containing the microfluidic channel (Harrick Plasma, PDC-32G).

A feedback-controlled fluid dispensing set up

The setup consists of a fluid level monitoring unit and a fluid control unit both synchronized through a Labview interface which has a user input for dispensing volume, as further depicted in Fig. S1.

The fluid monitoring unit consists of a capacitive fluid sensor which is capable of continuously monitoring the fluid level. In the fluid control unit, single layer valves which control the access of the fluid into the reaction chamber and waste channel are the key features. The pressure level in this dead-end channel, which dictates the degree of deformation of the valve, was regulated by a pressure pump (Fluigent, MFCS-EX). Rapid switching of the pressure level applied on the single-layer valves is critical to reducing their response time, this was achieved by the implementation of a three-way miniature diaphragm isolation valve (R9-312EP3L4P-000, Parker, USA) which was controlled by LabVIEW through an Arduino. The off-chip isolation valve could be switched to connect the on-chip single layer valve to a different pressure source, allowing rapid switching between degrees of membrane deformation.

Capacitive based fluid level monitoring hardware

The capacitance of the sensor was measured via capacitance to digital converter chip (AD7746, Analogue device), which has a dynamic detection range of ±4 pF with a precision of 4 fF. The data acquisition routine was implemented using an Adruino,[47] the single-ended mode of the AD7746 was used to maximize the detection range, and the capacitance was measured every 10 milliseconds and recorded through LabVIEW. A standard range extension circuit[48] was built to adjust the detection range according to the reagents used. To ensure that the detection range covers the input range and optimize the detection performance, the dynamical detection range was amplified 64 times, the bulk capacitance can be tuned according to the input range by setting on-chip digital-to-capacitance converter (CAPDAC).

Experimental Procedure

To initialize the experiment, the single-layer valves were prefilled with water to avoid the formation of the air bubbles during the pressurization of the valves. Then the system was cleaned with deionized (DI) water for 10 minutes followed by air drying to remove free ions and impurities which remained from fabrication. The reagent flow was applied, through the main channel with the valve controlling the waste outlet fully open, and the valve to the reaction chamber fully closed.

To perform the calibration process, the chamber is first filled and then emptied (by pressurizing the outlet). Here, by recording the capacitance values of the chamber when full and empty and by applying the linear relationship between fluid level and capacitance, the correlation between the fluid level and capacitive sensor was established. Further, this step pre-wets inlet to the reaction chamber, which prevents a building up of Young-Laplace pressure during the first dispensing step.

With calibration completed, the automated dispensing can commence. The fluid type can be altered in the main channel, with the target dispense volume entered into the user interface, the flow rate in the main channel was increased and the flow direction was diverted by closing the waste channel valve (1400 mbar) and partially opening the dispensing valve (by reducing the pressure from 1400 to 600 mbar). The fluid level was continuously monitored until the desired volume reached, at which point the dispensing valve was shut (1400 mbar), the waste channel valve opened (atmosphere), and the reagent flow rate reduced (pressure reduced to 10 mbar so lessening wastage).

SAW induced mixing was actuated when two different reagents had been added to the chamber. To test the capability of the capacitive sensor to detect mixing quality, benchmarking of this mixing needed to be performed using optical methods. To do this, a fresh fluorescent dye (fluorescein, Fluka Analytical) solution was added to fluorescent dye which had been photobleached in the chamber. The SAW was generated when an alternating electrical potential generated by an RF signal generator (Rohde & Schwarz, HAMEG HM8134-3) and then amplified (Amplifier Research, 25A250A) was applied to the IDTs. The capacitive monitoring of mixing quality was then assessed using different dilution of PBS.

The chip was placed on a Peltier cooler integrated into a 3D printed mount, with thermal contact being made using mineral oil. The Peltier cooler was actuated to keep the temperature on its surface at 19°C, this was monitored using a thermal camera (FLIR i7, FLIR Systems, Inc).

Data analysis

The experiments were conducted under a fluorescent optical microscope (Olympus BX43) recorded by CCD camera (PixeLink, PL-B872CU) video capture. The continuous capacitance monitoring on fluid level and mixing progress which benchmarked by fluorescent dye solution were analysed in Matlab. In the experiment conducted with transparent fluid (e.g. different concentrations of PBS buffer), automated optical analysis on the fluid level was hindered by background noise caused by the electrodes of the capacitive sensor. In assessing the fluid level visually, it is important to have an accurate determination of the channel geometry in the image, this was achieved by correlating the experimental bright field image with fluorescent reference image taken on the same chip with a chamber filled with fluorescein. In the cases that the chamber was only partially filled the air-fluid interface was determined manually, to avoid issues of the background noise.

4. Results and discussion

4.1. Fluid level tracking using a feedback loop

Firstly, the performance of the feedback control on regulating reagent dispensing was assessed in terms of the accuracy of the volume fed into the reaction chamber. This was

achieved using a comparison between two volume measuring techniques: optical and capacitive. A single fluid type was added, in stages, into the chamber. The initial dispensed volume was set to be 6.3 nL, then approximately doubled (the approximation coming from rounding of the required capacitance rather than system inaccuracy) to 12, 22, 40, and 78 nL, finally, the chamber was filled to 117 nL. A comparison of the optical and capacitive measurement of the dispensed volumes is given in Figure 2 (a), showing a very high level of accuracy, the error being in the range of 1 nL.

Although optical fluid level monitoring is widely used, the main limitation is associated with the fact that typically only one chamber/device can be monitored at one time. Further, to have enough contrast in the images to allow a fully automated and real-time analysis it is common to use of dyes and fluorophores. The first problem associated with the use of dyes is that not every chemical reaction is strictly compatible with their presence, and that long and continuous imaging can have collateral effects such as photo bleaching[49-50], photo toxicity[51] and photodegradation. Finally, we found that the contrast between newly added fluorescein and the one already present in the chamber during a long imaging session can be significantly greater than the contrast between the fluid and the background. This affects the accuracy of the optical measurements. The capacitance fluid level monitoring was significantly more robust, showing an ease of operation which makes it much more suitable for real time continuous monitoring. Further, being an electrical measurement it is easily compatible with multiplexing.

To demonstrate the robustness, accuracy and response of the dispensing automation, the process was repeated three times. Fig 2 (b) plotted the actual dispensed volume (both capacitive and optical) against the valve actuation threshold, showing the fast response of valve actuation and accuracy in fluid dispensing.

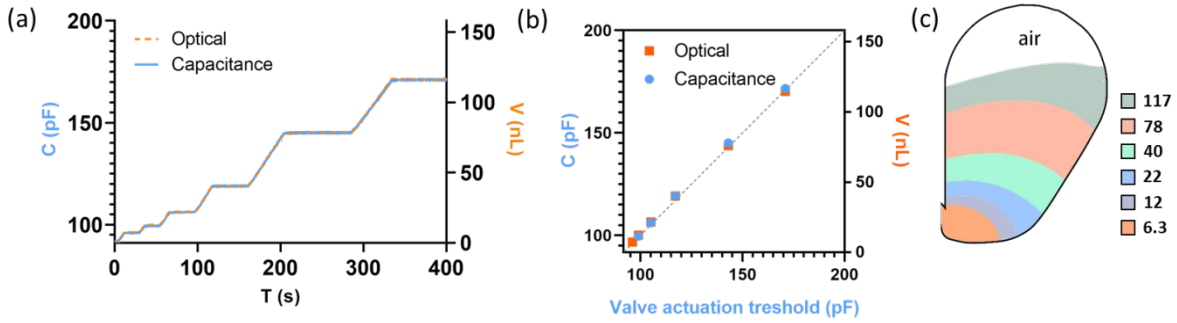

Figure 2 Dispensing of a single fluid type with feedback control. (a) Comparison between capacitance sensor readout and optical chamber reagent measurement on a single run of sequential fluid dispensing. The plot shows the agreement between the two fluid metering methods. (b) The accuracy of the dispensed versus target volume across three tests (error bar included). (c) A processed and layered image of the fluid volume at each filling stage.

4.2. Dispensing of Different fluids

In most applications reagents with different dielectric properties will need to be added and mixed. Here, we examine the functionality of the capacitive sensor for fluid volume control, when different fluid types are used. Firstly, the capacitance was measured as a function of PBS concentration, Fig. 3 (a), this demonstrates the strongly nonlinear relationship between concentration and measured capacitance (each time for a full chamber). However, this non-

linearity is not detrimental to the accuracy of dispensing. Indeed, by using capacitive change only, it does not need to be considered. The addition of fluid to the chamber is separate from mixing. So, the capacitance change will only be due to that caused by the added fluid, due to laminar flow dynamics upon dispensing, this will form a pocket of new fluid at the entrance of the chamber. In this unmixed state, the total capacitance is that of the initial fluid plus that of the added fluid, hence the capacitance difference is simply that of the added fluid. After dispensing the fluids will be mixed, and a new capacitance level reached due to the non-linearity seen in Fig 3 (a), but by this stage dispensing has been completed. For this to work there are a few conditions, firstly, the permittivity of any added fluid needs to be known, secondly, before the addition of new fluid the mixing of existing fluids in the chamber needs to be complete, and thirdly, the role of the conductivity needs to be removed by pre-wetting the chamber as described in the methodology section.

To demonstrate the addition of different fluid types, experiments were conducted in which PBS, a widely used biological buffer, was added sequentially into a chamber which initially was partly filled with a dilute PBS solution. Two different initial dilutions in water were used (25% and 50%). As the fluid added (at 100%) differs from the initial concentration, each sequential addition of fluid leads to a new overall concentration in the chamber.

As the diluted PBS was dispensed first, the capacitance sensor was calibrated by 25% and 50% PBS for the two experiments, respectively. After recording the capacitance value when the chamber is full the reagent was removed by the air pushing from the outlet and partial releasement of the dispensing valve. During this process of removing the reagent, as the surface of the substrate which is not completely hydrophobic, the surface charge was deposited over the entire surface of a capacitive sensor, removing issues caused by the charge in the double layer. It can be seen that even though at each step of the two experiments the initial concentration of PBS in the chamber will have been different, so the permittivity point on the curve in Fig. 3a will also be different, the use of only the capacitive changed during dispensing means that a very high level of accuracy is obtained (better than 2 nL in the worst case).

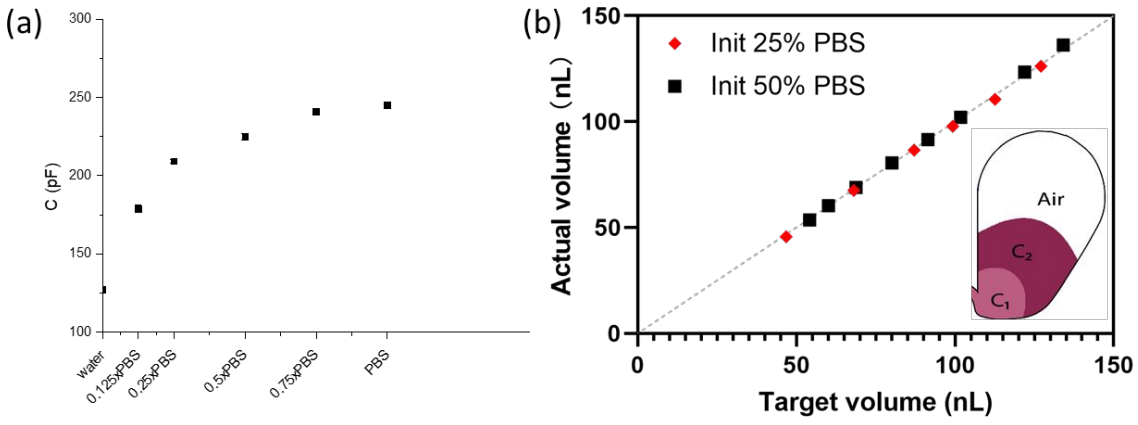

Figure 3 (a) Capacitance reading as function of PBS concentration at fluid level at 154 nL. (b)Comparison of theoretical estimation of sequential dispensing PBS based on capacitance reading (red) with optical measurement of experimental results (black).

4.3. Chamber Monitoring

The primary function of the capacitive sensor is to provide feedback on the dispensing of fluid, allowing, future, multiplexing of chambers outside the field of view of a microscope and bypassing issues around the need for fluorescent dye and its subsequent photobleaching. However, to operate chambers with no visual inspection, it would also be useful to be able to monitor temperature changes and mixing efficiency.

In actuating the surface acoustic wave-driven mixing, two unintentional effects can occur, atomization at the air-fluid interface and temperature rise. First, we examine the power limits which must be imposed to avoid atomisation, for this aspect of chamber monitoring we do not use the capacitive sensor, we simply visually gain data to impose operational limits. To examine atomisation, the mixing was observed optically by adding fresh fluorescein into the chamber which initially contains a photobleached sample. Photobleaching[50, 52] happens when the chemical structure of fluorophore been destructed. To mix the reagent effectively over the large area, SAW, with a frequency of 70 MHz frequency, was applied.

The time is taken to mix the fluids varies with the ratio of the volume of reagents being mixed. The ability of precise control reagent volume enables quantification of this variation. Fig.4 (a), shows that for a constant fluid level 154 nL, using a SAW actuation power of 0.26 W, the mixing time increases from 23s to 26 s when the mixing ratio varies from 1:1 to 1:4.

Atomization[53] occurs when significant wave amplitude impinges on the air-fluid interface, resulting in a fine mist of spray during mixing. As the SAW amplitude attenuates when the wave propagates under a fluid (due to energy coupling into the fluid, which drives the mixing), this effect is more pertinent when dealing with small volumes of fluid. As such, to avoid loss of sample, the SAW power applied needs to be limited according to the fluid level. Fig.4 (b) shows the mixing time across different volumes ranging from 6 nL to 154 nL, in each case two fluids of equal volume were mixed. The maximum SAW power applied before the onset of atomisation can be seen to increase very significantly as the volume is increased, noting the length of the chamber in the direction of SAW propagation is 30 times its wavelength. As a result of the power limits this imposes, it can be seen that the mixing time ranging from 22 s to 38 s, with the medium fluid level taking the longest.

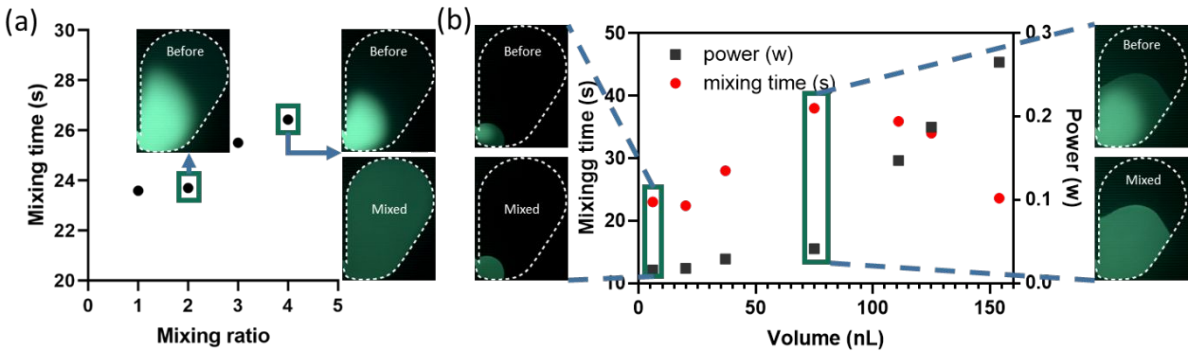

Figure 4 (a) Effect of different mixing ratio on mixing time for 154 nL, with constant power 0.26 W applied (b). Mixing time (black) on varies volume and corresponding SAW excitation power (red).

The capacitive sensor can be used to measure the second adverse effect that of temperature rise. We examine the measurement of this for the case of mixing in a full chamber, as under this condition the maximum power can be applied. Although a thermal camera or thermostat

can provide sensitive temperature measurement, accurately monitoring of the local temperature inside the microfluidic chamber is challenging due to the localized and transient heating caused by the SAW propagation and the poor thermal conduction of both $LiNbO_3$ substrate and the PDMS channel. As such, the capacitive sensor, embedded under the reaction chamber and directly in contact with reaction fluid has the potential to provide much better accuracy in monitoring temperature change.

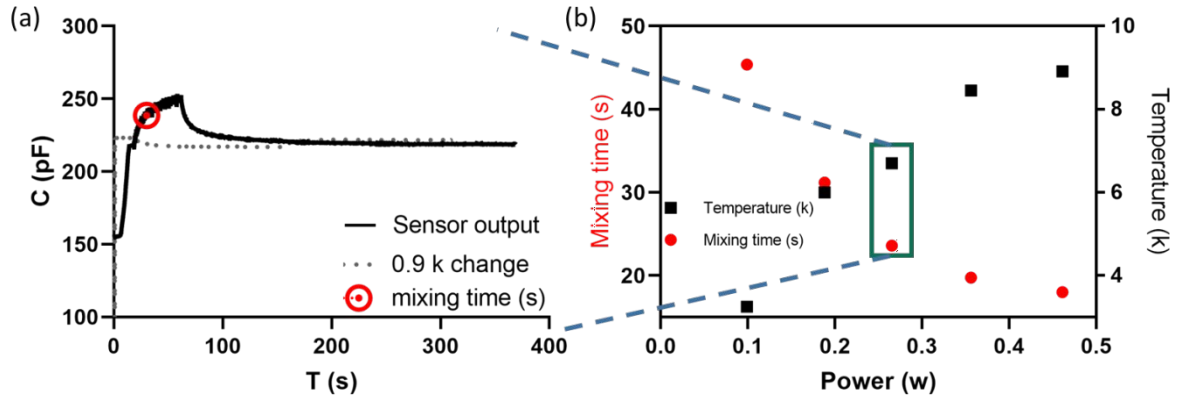

Figure 5 Mixing characterization. (a)Capacitance change during one mixing case, fresh fluorescein was added in, feeding channel shut. SAW was actuated for mixing, after visualize mixing process complete, the SAW was turned off. (b) Mixing time (red) as well as temperature (black) change against power.

Figure 5(a) shows the capacitance readout during the mixing process for one experiment. Initially, the chamber is half-filled with photobleached fluorescein solution, then the dispensing valve opens, and the capacitance increases significantly as the fresh fluorescein is added into the chamber. When dispensing is complete the capacitance value levels off (at 14 s). The next increase (18 s to 62 s) occurs during the SAW actuation. Because the two fluids are chemically identical, this increase is due solely to temperature increase. Once the SAW is turned off, the capacitance reading drops to previous value as the heat was dissipated. Through image analysis, the mixing time was determined (red dot). The increase in capacitance reading due to temperature change when the mixing is complete was obtained. Comparing the capacitance change caused by a decrease in temperature of 0.9 K (shown by the grey dashed line) and based on a linear relationship,[54] we were able to calculate the temperature change dependent on the SAW actuation.

Whilst the temperature change is monitored, the mixing time is found for a range of SAW powers, in each case for a full chamber, as shown in Fig.5(b). As the power is increased from 0.1 W to 0.4 W, the mixing time was reduced from 45 s to 18 s, but the temperature change increased from 3.2 K to 8.9 K. Although the mixing is faster when higher powers are used the chamber is also heated faster. By using the capacitive sensor to quantify these effects, the operating power can be selected to optimally balance the mixing time and the effects of heating. Accordingly, we found that 0.26 W reduces by 7.6 s the mixing time when compared to 0.19 W while the temperature raises by only 0.7 K. The data shows that for the mixing temperature-insensitive sample, more power can be applied to reduce mixing time to 18s.

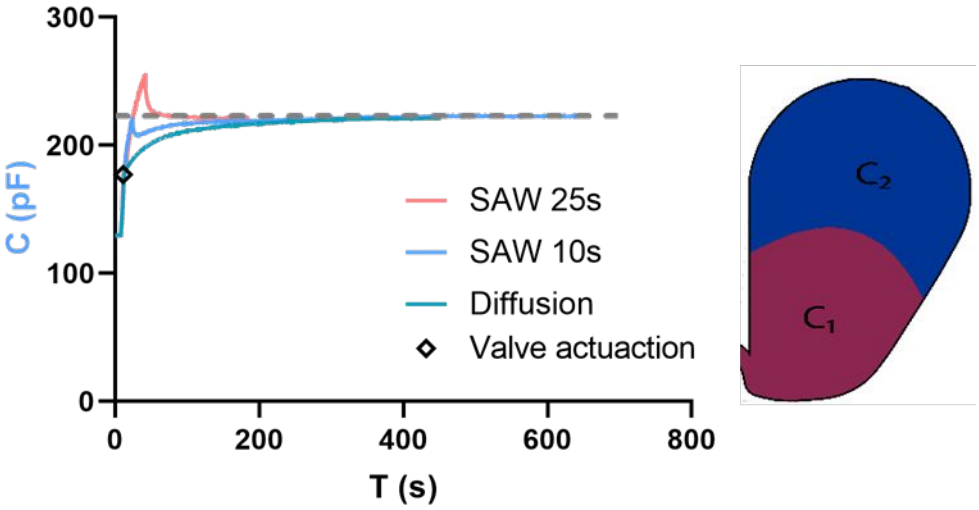

Figure 6 Comparison of capacitance readout for mixing fluid with different conductivity (PBS and 50% diluted PBS), when it is fully mixed (SAW actuation=25 s), under mixed (SAW actuation=10s) and passive control (diffusion)

When two different fluids are added, the capacitance of the mixed state will be different from the sum of the capacitance from the two unmixed states, due to the non-linearity shown in Fig. 4 (a). This allows for monitoring the mixing performance. Fig. 6 shows the capacitance readout overtime in three experiments, in the first no active mixing is used, and in the second two, a burst of SAW for 10 and 25 s is used. At the power used, 0.26 W, the data in Fig. 6 (a) shows that 25 s is adequate for full mixing, whilst 10 s is not. In each case, the chamber contains half PBS and half a solution of PBS at 50% concentration. Once the fluids were dispensed (shown with a black rhombus), the capacitance change is due to the mixing. For the diffusion case, it can be seen that there is a gradual increase until a stable value (variation of <1.5% thereafter) is reached at 420 s. Whilst for the case of the 25 s of SAW, there is a sharp rise in capacitance, due to the temperature rise (characterised in Fig 6), and then as the heat dissipates the capacitance falls and a steady value for the mixed fluid is reached from above after 74 s. For the case of inadequate SAW actuation, 10 s, the same temperature spike occurs, but then the capacitance falls below the fully mixed value, and only rises at the timescale of diffusion, reaching the final value from below at 303 s. The length of time required for mixing can, therefore, be characterised by the capacitance curves, with no need for fluorescein, and optical access.

5. Conclusion

We have demonstrated an automated system with multiplexing potential for performing protocols on-chip with nanolitre dispensing flexibility, SAW aided rapid mixing and capacitive sensing for fluid level, temperature and mixing progress monitoring. Versatile nanolitre dispensing was achieved via incorporating capacitive fluid level sensor and control algorithm for single layer valve operation, dispense accuracy was examined by sequential dispense single fluid and multiple fluids respectively, results showing accuracy within 2 nL. The precise control of dispensing and versatile measurement of capacitive sensing for chamber

monitoring enabled in-depth characterisation for SAW aided mixing. The variation of mixing time due to change in mixing ratio was investigated, an increase of mixing time from 23s to 26s when change in mixing ratio from 1:1 to 1:4 was found for 154 nL at excitation power of 0.26 W. For volume ranging from 6 nL to 154 nL, cut-off excitation power varies with fluid volume to avoid sample loss. The temperature change associated with power applied was examined when the chamber was filled, with an increase of the power from 0.1 W to 0.46 W, mixing time was reduced to 45s to 18s while temperature increased from 3.2 K to 8.9 K. Lastly, after the characterisation on SAW mixing capability, we demonstrated the capacitive sensing for mixing progress monitoring by comparing capacitance readout with optical measurements with (25s), insufficient SAW actuation (10s) and passive control. The capacitance readout showed agreement with optical measurement, providing a compact versatile monitoring method allowing direct sensing that avoids the need for bulky optical measurement and offers potential for multiplexing.

Acknowledgements

The fabrication required for this work was performed in part at the Melbourne Centre for Nanofabrication (MCN) in the Victorian Node of the Australian National Fabrication Facility (ANFF).

Reference

1. Elvira, K. S.; i Solvas, X. C.; Wootton, R. C. R.; deMello, A. J., The past, present and potential for microfluidic reactor technology in chemical synthesis. *Nature Chemistry* **2013,** *5* (11), 905-915.
2. Heath, J. R.; Ribas, A.; Mischel, P. S., Single-cell analysis tools for drug discovery and development. *Nature Reviews Drug Discovery* **2016,** *15* (3), 204-216.
3. Dey, S. S.; Kester, L.; Spanjaard, B.; Bienko, M.; Van Oudenaarden, A., Integrated genome and transcriptome sequencing of the same cell. *Nature biotechnology* **2015,** *33* (3), 285-289.
4. Macaulay, I. C.; Haerty, W.; Kumar, P.; Li, Y. I.; Hu, T. X.; Teng, M. J.; Goolam, M.; Saurat, N.; Coupland, P.; Shirley, L. M., G&T-seq: parallel sequencing of single-cell genomes and transcriptomes. *Nature methods* **2015,** *12* (6), 519.
5. Budnik, B.; Levy, E.; Harmange, G.; Slavov, N., SCoPE-MS: mass spectrometry of single mammalian cells quantifies proteome heterogeneity during cell differentiation. *Genome biology* **2018,** *19* (1), 161.
6. Lignos, I.; Stavrakis, S.; Nedelcu, G.; Protesescu, L.; deMello, A. J.; Kovalenko, M. V., Synthesis of Cesium Lead Halide Perovskite Nanocrystals in a Droplet-Based Microfluidic Platform: Fast Parametric Space Mapping. *Nano Letters* **2016,** *16* (3), 1869-1877.
7. Maceiczyk, R. M.; Dümbgen, K.; Lignos, I.; Protesescu, L.; Kovalenko, M. V.; deMello, A. J., Microfluidic Reactors Provide Preparative and Mechanistic Insights into the Synthesis of Formamidinium Lead Halide Perovskite Nanocrystals. *Chemistry of Materials* **2017,** *29* (19), 8433-8439.
8. Macosko, Evan Z.; Basu, A.; Satija, R.; Nemesh, J.; Shekhar, K.; Goldman, M.; Tirosh, I.; Bialas, Allison R.; Kamitaki, N.; Martersteck, Emily M.; Trombetta, John J.; Weitz, David A.; Sanes, Joshua R.; Shalek, Alex K.; Regev, A.; McCarroll, Steven A., Highly Parallel Genome-wide Expression Profiling of Individual Cells Using Nanoliter Droplets. *Cell* **2015,** *161* (5), 1202-1214.
9. Suea-Ngam, A.; Howes, P. D.; Srisa-Art, M.; deMello, A. J., Droplet microfluidics: from proof-of-concept to real-world utility? *Chemical Communications* **2019,** *55* (67), 9895-9903.
10. Chiu, D. T.; deMello, A. J.; Di Carlo, D.; Doyle, P. S.; Hansen, C.; Maceiczyk, R. M.; Wootton, R. C. R., Small but Perfectly Formed? Successes, Challenges, and Opportunities for Microfluidics in the Chemical and Biological Sciences. *Chem* **2017,** *2* (2), 201-223.

11. Sesen, M.; Alan, T.; Neild, A., Droplet control technologies for microfluidic high throughput screening (μHTS). *Lab on a Chip* **2017,** *17* (14), 2372-2394.
12. Streets, A. M.; Zhang, X.; Cao, C.; Pang, Y.; Wu, X.; Xiong, L.; Yang, L.; Fu, Y.; Zhao, L.; Tang, F., Microfluidic single-cell whole-transcriptome sequencing. *Proceedings of the National Academy of Sciences* **2014,** *111* (19), 7048-7053.
13. White, A. K.; VanInsberghe, M.; Petriv, O. I.; Hamidi, M.; Sikorski, D.; Marra, M. A.; Piret, J.; Aparicio, S.; Hansen, C. L., High-throughput microfluidic single-cell RT-qPCR. *Proceedings of the National Academy of Sciences* **2011,** *108* (34), 13999-14004.
14. Hong, J. W.; Studer, V.; Hang, G.; Anderson, W. F.; Quake, S. R., A nanoliter-scale nucleic acid processor with parallel architecture. *Nature biotechnology* **2004,** *22* (4), 435.
15. Lee, C.-C.; Sui, G.; Elizarov, A.; Shu, C. J.; Shin, Y.-S.; Dooley, A. N.; Huang, J.; Daridon, A.; Wyatt, P.; Stout, D.; Kolb, H. C.; Witte, O. N.; Satyamurthy, N.; Heath, J. R.; Phelps, M. E.; Quake, S. R.; Tseng, H.-R., Multistep Synthesis of a Radiolabeled Imaging Probe Using Integrated Microfluidics. *Science* **2005,** *310* (5755), 1793-1796.
16. Warren, L.; Bryder, D.; Weissman, I. L.; Quake, S. R., Transcription factor profiling in individual hematopoietic progenitors by digital RT-PCR. *Proceedings of the National Academy of Sciences* **2006,** *103* (47), 17807-17812.
17. Thorsen, T.; Maerkl, S. J.; Quake, S. R., Microfluidic large-scale integration. *Science* **2002,** *298* (5593), 580-584.
18. Jr., F. R. P.; Hughes, N. R.; Pathak, J. A., Chaotic mixing in microfluidic devices driven by oscillatory cross flow. *Physics of Fluids* **2008,** *20* (2), 023101.
19. Hess, D.; Rane, A.; deMello, A. J.; Stavrakis, S., High-Throughput, Quantitative Enzyme Kinetic Analysis in Microdroplets Using Stroboscopic Epifluorescence Imaging. *Analytical Chemistry* **2015,** *87* (9), 4965-4972.
20. Unger, M. A.; Chou, H.-P.; Thorsen, T.; Scherer, A.; Quake, S. R., Monolithic microfabricated valves and pumps by multilayer soft lithography. *Science* **2000,** *288* (5463), 113-116.
21. Abate, A.; Weitz, D., Single-layer membrane valves for elastomeric microfluidic devices. *Applied Physics Letters* **2008,** *92* (24), 243509.
22. Abate, A. R.; Agresti, J. J.; Weitz, D. A., Microfluidic sorting with high-speed single-layer membrane valves. *Applied Physics Letters* **2010,** *96* (20), 203509.
23. Abate, A. R.; Romanowsky, M. B.; Agresti, J. J.; Weitz, D. A., Valve-based flow focusing for drop formation. *Applied Physics Letters* **2009,** *94* (2), 023503.
24. Zhang, Y.; Devendran, C.; Lupton, C.; de Marco, A.; Neild, A., Versatile platform for performing protocols on a chip utilizing surface acoustic wave (SAW) driven mixing. *Lab on a Chip* **2019,** *19* (2), 262-271.
25. Soenksen, L. R.; Kassis, T.; Noh, M.; Griffith, L. G.; Trumper, D. L., Closed-loop feedback control for microfluidic systems through automated capacitive fluid height sensing. *Lab on a Chip* **2018,** *18* (6), 902-914.
26. Temiz, Y.; Delamarche, E., Sub-nanoliter, real-time flow monitoring in microfluidic chips using a portable device and smartphone. *Scientific reports* **2018,** *8* (1), 10603.
27. Elbuken, C.; Glawdel, T.; Chan, D.; Ren, C. L., Detection of microdroplet size and speed using capacitive sensors. *Sensors and Actuators A: Physical* **2011,** *171* (2), 55-62.
28. Chen, J. Z.; Darhuber, A. A.; Troian, S. M.; Wagner, S., Capacitive sensing of droplets for microfluidic devices based on thermocapillary actuation. *Lab on a Chip* **2004,** *4* (5), 473-480.
29. Isgor, P. K.; Marcali, M.; Keser, M.; Elbuken, C., Microfluidic droplet content detection using integrated capacitive sensors. *Sensors and Actuators B: Chemical* **2015,** *210*, 669-675.
30. Sesen, M.; Devendran, C.; Malikides, S.; Alan, T.; Neild, A., Surface acoustic wave enabled pipette on a chip. *Lab on a Chip* **2017,** *17* (3), 438-447.
31. Demori, M.; Ferrari, V.; Poesio, P.; Strazza, D., A microfluidic capacitance sensor for fluid discrimination and characterization. *Sensors and Actuators A: Physical* **2011,** *172* (1), 212-219.

32. Nyborg, W. L., Acoustic streaming due to attenuated plane waves. *The journal of the acoustical society of America* **1953,** *25* (1), 68-75.
33. Nam, J.; Jang, W. S.; Lim, C. S., Micromixing using a conductive liquid-based focused surface acoustic wave (CL-FSAW). *Sensors and Actuators B: Chemical* **2018,** *258*, 991-997.
34. Ozcelik, A.; Rufo, J.; Guo, F.; Gu, Y.; Li, P.; Lata, J.; Huang, T. J., Acoustic tweezers for the life sciences. *Nature Methods* **2018,** *15* (12), 1021-1028.
35. Alghane, M.; Fu, Y. Q.; Chen, B.; Li, Y.; Desmulliez, M. P. Y.; Walton, A., Frequency effect on streaming phenomenon induced by Rayleigh surface acoustic wave in microdroplets. *Journal of Applied Physics* **2012,** *112* (8), 084902.
36. Devendran, C.; Albrecht, T.; Brenker, J.; Alan, T.; Neild, A., The importance of travelling wave components in standing surface acoustic wave (SSAW) systems. *Lab on a Chip* **2016,** *16* (19), 3756-3766.
37. Lighthill, S. J., Acoustic streaming. *Journal of Sound and Vibration* **1978,** *61* (3), 391-418.
38. Ahmed, D.; Mao, X.; Shi, J.; Juluri, B. K.; Huang, T. J., A millisecond micromixer via single-bubble-based acoustic streaming. *Lab on a Chip* **2009,** *9* (18), 2738-2741.
39. Zhou, W.; Niu, L.; Cai, F.; Li, F.; Wang, C.; Huang, X.; Wang, J.; Wu, J.; Meng, L.; Zheng, H., Spatial selective manipulation of microbubbles by tunable surface acoustic waves. *Biomicrofluidics* **2016,** *10* (3), 034121.
40. Liu, R. H.; Yang, J.; Pindera, M. Z.; Athavale, M.; Grodzinski, P., Bubble-induced acoustic micromixing. *Lab on a Chip* **2002,** *2* (3), 151-157.
41. Ozcelik, A.; Ahmed, D.; Xie, Y.; Nama, N.; Qu, Z.; Nawaz, A. A.; Huang, T. J., An Acoustofluidic Micromixer via Bubble Inception and Cavitation from Microchannel Sidewalls. *Analytical Chemistry* **2014,** *86* (10), 5083-5088.
42. Huang, P.-H.; Xie, Y.; Ahmed, D.; Rufo, J.; Nama, N.; Chen, Y.; Chan, C. Y.; Huang, T. J., An acoustofluidic micromixer based on oscillating sidewall sharp-edges. *Lab on a Chip* **2013,** *13* (19), 3847-3852.
43. Bachman, H.; Chen, C.; Rufo, J.; Zhao, S.; Yang, S.; Tian, Z.; Nama, N.; Huang, P.-H.; Huang, T. J., An acoustofluidic device for efficient mixing over a wide range of flow rates. *Lab on a Chip* **2020,** *20* (7), 1238-1248.
44. Van Phan, H.; Coşkun, M. B.; Şeşen, M.; Pandraud, G.; Neild, A.; Alan, T., Vibrating membrane with discontinuities for rapid and efficient microfluidic mixing. *Lab on a Chip* **2015,** *15* (21), 4206-4216.
45. Stern, E.; Wagner, R.; Sigworth, F. J.; Breaker, R.; Fahmy, T. M.; Reed, M. A., Importance of the Debye Screening Length on Nanowire Field Effect Transistor Sensors. *Nano Letters* **2007,** *7* (11), 3405-3409.
46. Nie, B.; Li, R.; Cao, J.; Brandt, J. D.; Pan, T., Flexible Transparent Iontronic Film for Interfacial Capacitive Pressure Sensing. *Advanced Materials* **2015,** *27* (39), 6055-6062.
47. Devices, A. Analog Devices AD7746: 24-bit, 2 Channel Capacitance to Digital Converter. (accessed 2010).
48. devices, A. Extending the Capacitive Input Range of the AD7745/AD7746 Capacitance-to-Digital Converter.
49. Song, L.; Hennink, E. J.; Young, I. T.; Tanke, H. J., Photobleaching kinetics of fluorescein in quantitative fluorescence microscopy. *Biophysical Journal* **1995,** *68* (6), 2588-2600.
50. Saylor, J., Photobleaching of disodium fluorescein in water. *Experiments in fluids* **1995,** *18* (6), 445-447.
51. Kochevar, I. E., Phototoxicity Mechanisms: Chlorpromazine Photosensitized Damage to DNA and Cell Membranes. *Journal of Investigative Dermatology* **1981,** *77* (1), 59-64.
52. Song, L.; Hennink, E.; Young, I. T.; Tanke, H. J., Photobleaching kinetics of fluorescein in quantitative fluorescence microscopy. *Biophysical journal* **1995,** *68* (6), 2588-2600.
53. Ashtiani, D.; de Marco, A.; Neild, A., Tailoring surface acoustic wave atomisation for cryo-electron microscopy sample preparation. *Lab on a Chip* **2019,** *19* (8), 1378-1385.

54. Ha, B. H.; Lee, K. S.; Destgeer, G.; Park, J.; Choung, J. S.; Jung, J. H.; Shin, J. H.; Sung, H. J., Acoustothermal heating of polydimethylsiloxane microfluidic system. *Scientific reports* **2015,** *5*, 11851-11851.

TOC Graphic

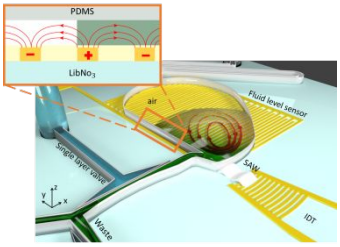
PDMS
LiNbO3
air
Fluid level sensor
Sample inlet valve
SAW
IDT
Waste